Spin excitations arising from anisotropic Dirac spinons in $YCu_3(OD)_6Br_2[Br_{0.33}(OD)_{0.67}]$

Lankun Han,[1,2] Zhenyuan Zeng,[1,2] Bo Liu,[1] Maiko Kofu,[3] Kenji Nakajima,[3,*] Paul Steffens,[4] Arno Hiess,[4] Yixi Su,[5,†] and Shiliang Li[1,2,‡]

[1] *Beijing National Laboratory for Condensed Matter Physics, Institute of Physics, Chinese Academy of Sciences, Beijing 100190, China*
[2] *School of Physical Sciences, University of Chinese Academy of Sciences, Beijing 100190, China*
[3] *J-PARC Center, Japan Atomic Energy Agency, Tokai, Japan*
[4] *Institut Laue-Langevin, 71 Avenue des Martyrs, 38000 Grenoble, France*
[5] *Jülich Centre for Neutron Science (JCNS) at Heinz Maier-Leibnitz Zentrum (MLZ), Forschungszentrum Jülich, Lichtenbergstrasse 1, 85747 Garching, Germany*

A Dirac quantum spin liquid hosts Dirac spinons, which are low-energy fractionalized neutral quasiparticles with spin 1/2 that obey the Dirac equation. Recent studies have revealed cone spin continuum in $YCu_3(OD)_6Br_2[Br_x(OD)_{1-x}]$, consistent with the convolution of two Dirac spinons. In this work, we further studied spin excitations using the inelastic neutron scattering technique. The width of low-energy spin excitations shows a linear temperature dependence, which can be explained by spinon-spinon interactions with a Dirac dispersion. Polarized neutron scattering measurements reveal that in-plane magnetic fluctuations are about 1.5 times stronger than the out-of-plane ones, suggesting the presence of out-of-plane Dzyaloshinskii-Moriya interaction. Moreover, the high-energy spin excitations around 14 meV agree with the one-pair spinon-antispinon excitations in Raman studies. The real part of the dynamical susceptibility derived from the Kramers-Kronig relationship also accords with the Knight shift measured by nuclear magnetic resonance. These results provide further insights for the possible Dirac quantum spin liquid in this system.

A Dirac spinon is a kind of fractionalized excitations in quantum spin liquids (QSLs) that has been widely discussed in theories [1–3]. A Dirac spinon has spin 1/2 and is described by the Dirac equation, i.e., it is a fermion with linear dispersion, analogous to electrons in graphene but without the charge degree of freedom. One of the most promising models to study Dirac spinons is the antiferromagnetic (AFM) Heisenberg model on the kagome lattice [4–16]. Despite theoretical triumphs, the search for Dirac QSLs in the kagome materials has largely failed. One of the main reasons may be the existence of disorders and magnetic impurities in these materials [17–29], which may blur the sharp features of low-energy spin excitations in a Dirac QSL or even destroy it.

Recently, a new kagome system, $YCu_3(OH)_6Br_2[Br_{1-x}(OH)_x]$ (YCu_3-Br), has shown many interesting results that make it a promising QSL candidate [30–39]. Unlike many other kagome QSL candidates, this system shows no sign of magnetic impurities or weakly correlated spins. Heat capacity measurements clearly reveal behaviors expected for a Dirac QSL, including the quadratic temperature dependence of the specific heat at zero field and a linear term under fields [31]. More intriguingly, the spin excitations show cone continuum that may come from the convolution of two Dirac spinons [36]. These results show no sign of disorders and impurities, making YCu_3-Br the best candidate for the Dirac QSL so far. However, there are also several results that do not favor or even go against the existence of Dirac spinons. Thermal conductivity measurements do not observe a linear term that is supposed to exist in the presence of spinon Fermi surfaces coming from the Dirac spinons under fields [33]. Moreover, magnetic susceptibility shows almost no temperature dependence at low temperatures [31, 35, 40], whereas a linear temperature dependence is expected for a Dirac QSL. These results cast a shadow over the existence of Dirac spinons and has aroused alternate explanations [39]. It is worth noting that a one-ninth magnetization plateau and magnetic oscillations have been observed at about 20 T, and their origin is also debated [40–43].

In this work, we studied the spin excitations of $YCu_3(OD)_6Br_2[Br_{0.33}(OD)_{0.67}]$ using the inelastic neutron scattering (INS) technique. The temperature dependence and anisotropy of the low-energy spin excitations suggest finite quasiparticle lifetimes and the existence of Dzyaloshinskii-Moriya (DM) interaction. We argue that these factors explain the negative results from thermal conductivity and magnetic susceptibility measurements. Moreover, the dynamical susceptibility agrees excellently with Raman and NMR results, providing further evidence of the Dirac QSL in this system.

Single crystals of $YCu_3(OD)_6Br_2[Br_{0.33}(OD)_{0.66}]$ were grown using the hydrothermal method as reported previously [31]. Since the sample properties may vary among different batches [37]. we have measured the low-temperature specific heats of the samples from all batches to make sure that the crystals used in the INS measurements exhibit the same properties [44]. About 800 single crystals with a mass of approximate 0.5 gram were co-aligned on a Cu plate using CYTOP, with a mosaic spread of about 3 degrees [44]. The momentum trans-

fer Q in three-dimensional reciprocal space is defined as $Q = H\mathbf{a}^*+K\mathbf{b}^*+L\mathbf{c}^*$, where H, K and L are Miller indices and $\mathbf{a}^* = 2\pi(\mathbf{b}\times\mathbf{c})/\mathrm{V}$, $\mathbf{b}^* = 2\pi(\mathbf{c}\times\mathbf{a})/\mathrm{V}$ and $\mathbf{c}^* = 2\pi(\mathbf{a}\times\mathbf{b})/\mathrm{V}$, with a = b = 6.6779 Å, c = 5.9874 Å, and V = 231.23 Å^3 of the kagome lattice. The crystal assembly was aligned in the [H, 0, L] scattering plane. The unpolarized and polarized INS experiments were carried out on the cold-neutron disk chopper spectrometer AMATERAS at J-PARC [45] and the cold-neutron triple-axis spectrometer ThALES at ILL [46], respectively. All the spectral data of AMATERAS were processed by using the software suite Utsusemi [47]. In the polarized neutron experiment, an XYZ coil system is used for providing the needed guide fields at the sample, and the incoming neutron polarization directions are denoted as x, y, and z with x along the Q direction. While both y and z are perpendicular to Q, they are within and perpendicular to the scattering plane, respectively. After scattered by the sample, the outgoing neutron polarization can either parallel or antiparallel to the incoming neutron polarization, which corresponds to the nonspin flip (NSF) and spin flip (SF) processes, respectively.

As shown in our previous work [36], the spin excitations of YCu_3-Br exhibit cone continua at six symmetrical positions within one Brillouin zone, among which the one at (2/3,0) has the strongest intensity. Figures 1(a) and 1(b) show the colormaps of the low-energy spin excitations as a function of E and Q along the [H,0] direction at 0.3 and 6 K, respectively. Similar to previous results, the cone continuum is clearly revealed at both (2/3,0) and (4/3,0) at 0.3 K. At 6 K, the cone continuum becomes column-like due to the significant broadening of low-energy spin excitations.

Figures 1(c) and 1(d) show constant-E cuts at 0.1 and 0.5 meV, respectively, all of which can be well fitted by the Lorentzian function. The obtained energy and temperature dependence of FWHM are shown in Figs. 1(c) and 1(d), respectively. The FWHM changes linearly with E at low temperatures. The slope at 0.3 K is 0.191 ± 0.011 eVÅ, which is slightly larger than the value reported previously [36]. This accords with the fact that previous INS measurements used samples with various T^2 coefficients in the specific heat [37], which are directly associated with the widths of the spin excitations for a Dirac QSL [36]. Interestingly, the FWHM at 0.1 meV also changes linearly with T up to 6 K, with a slope of about 0.0211 ± 0.003 Å^{-1}/K, while those above 0.5 meV show little temperature dependence.

To further reveal the nature of the low-energy spin excitations, we also carried out polarized INS measurements in the [H,0,L] plane, as illustrated in Fig. 2(a). Since neutrons only detect magnetic scattering components perpendicular to Q, we can obtain magnetic responses along the y and z directions, denoted as M_y and

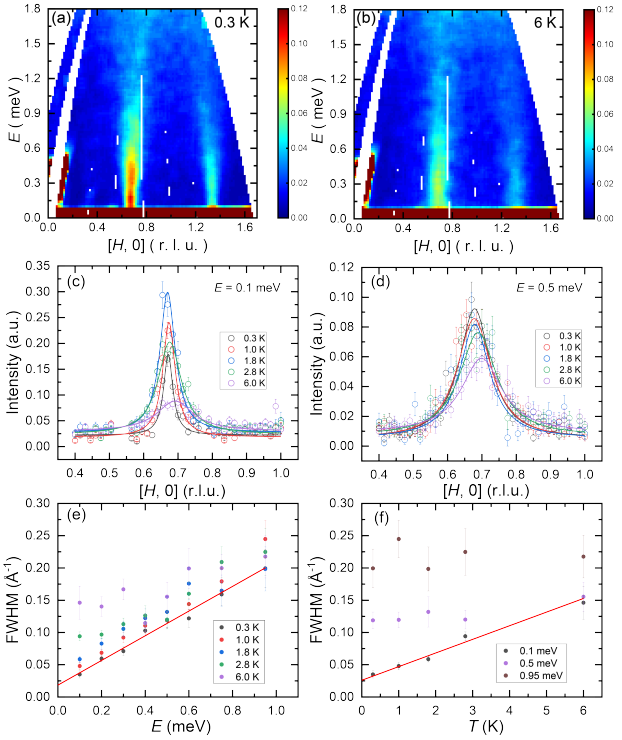

FIG. 1. (a) and (b) Intensity contour plots of the INS results as a function of E and Q along the [H,0] direction at 0.3 and 6 K, respectively, with E_i = 2.57 meV. (c) and (d) Constant-E cuts along the [H,0] direction at 0.1 and 0.5 meV, respectively. The solid lines are fitted results by the Lorentzian function. The integrated ranges of the energy and [-0.5K, K] are ± 0.05 meV and ± 0.1 r.l.u., respectively. (e) and (f) Energy and temperature dependence of the FWHM. The solid lines in (c) and (d) are results of linear fits at 0.3 K and 0.1 meV, respectively. In all figures, r.l.u. is the reciprocal lattice unit.

M_z, respectively. Accordingly [48], we obtain

$$M_y = \frac{R+1}{R-1}(\sigma_x^{SF} - \sigma_y^{SF}), \quad (1)$$

$$M_z = \frac{R+1}{R-1}(\sigma_x^{SF} - \sigma_z^{SF}), \quad (2)$$

where σ_x^{SF}, σ_y^{SF}, and σ_z^{SF} are the SF scattering cross sections for the corresponding neutron polarization direction, and R is the flipping ratio between NSF and SF scattering. R is large (> 15) so the flipping-ratio correction term can be neglected. As shown in Fig. 2(b), for magnetic intensities of excitations within the ab plane (M_{ab}) and along the c axis (M_c), we obtain $M_z = M_{ab}$ and $M_y = M_{ab}sin^2\theta + M_c cos^2\theta$, where θ is the angle between Q and the (H,0,0) direction. Here, we focus on the spin excitations at 0.2 meV and 50 mK around (2/3,0,0). Figures 2(c) and 2(d) show scans along the [H,0,0] and [2/3,0,L] directions for all three SF channels, respectively. The corresponding M_{ab} and M_c can thus be obtained as shown in Figs. 2(e) and 2(f). In both cases, the ratio of M_{ab}/M_c is very close to 1.5. We note

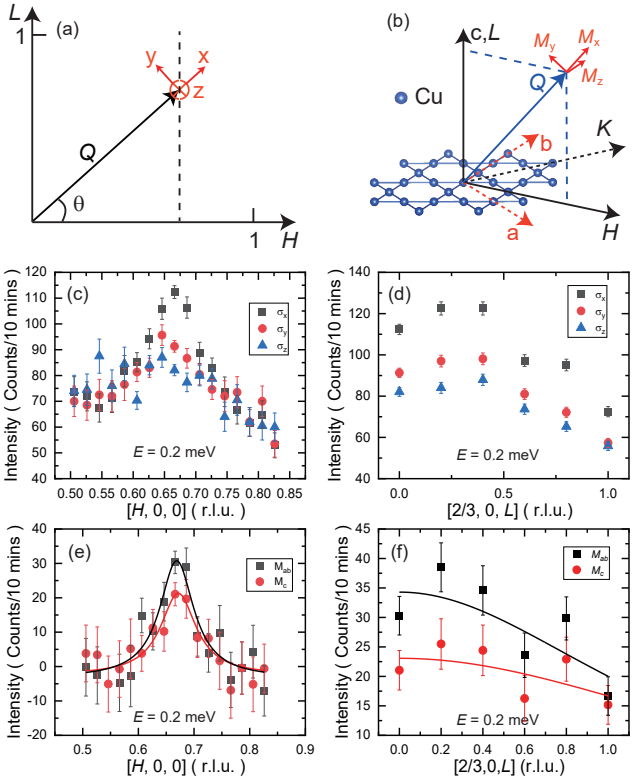

FIG. 2. (a) and (b) Illustration of the neutron polarized measurement in the $[H,0,L]$ plane and real space. The x, y, and z are the neutron polarization directions. The angle between Q and the $(H,0,0)$ direction is denoted as θ. (c), (d) Constant-E scans at 0.2 meV along the $[H,0,0]$ and $[2/3,0,L]$ directions, respectively. (e), (f) In-plane and out-of-plane magnetic responses (M_{ab} and M_c) at 0.2 meV along the $[H,0,0]$ and $[2/3,0,L]$ directions, respectively. The solid lines in (e) are fitted by a Lorentzian functiont. The solid lines in (f) are guides by the eye. All measurements in this figure were carried out at about 50 mK and with a fixed $k_f = 1.3$ Å^{-1} .

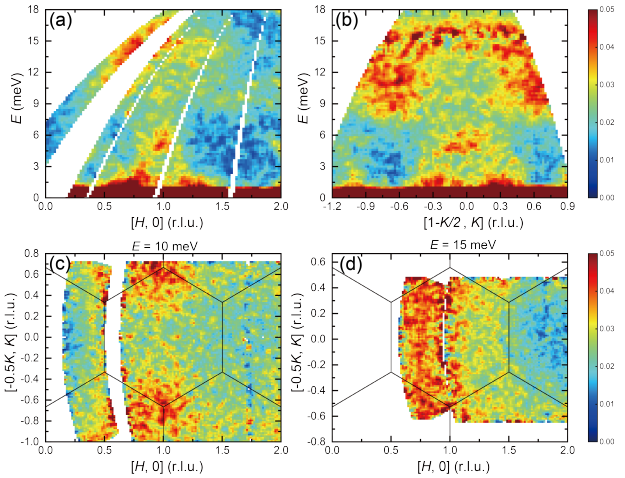

FIG. 3. (a) and (b) Intensity contour plots of the INS results as a function of E and Q along the $[H,0]$ and $[1\text{-}K/2,K]$ directions, respectively, with $E_i = 21.91$ meV and $T = 0.3$ K. The corresponding integrated range along the $[\text{-}K/2,\ K/2]$ and $[H,0]$ directions are from K = -0.12 to K = 0.12 and from $H = 0.9$ to $H = 1.1$, respectively. (c) Intensity contour plot of the INS results within the $[H,K]$ plane at 10 and 15 meV, respectively, at $T = 0.3$ K. The integrated energy range is 2 meV. The solid lines are the kagome Brillouin zone.

that this anisotropy can not be due to the anisotropic g-factor since g_{ab}/g_c is slightly smaller than 1 as shown by the magnetization measurements [31, 42].

In the following, we turn to the results of high-energy spin excitations. Figures 3(a) and 3(b) show high-energy spin excitations at 0.3 K along the $[H,0]$ and $[1\text{-}K/2,K]$ directions, respectively. In previous studies, the spin excitations were observed up to about 8 meV due to the incident energy limit [36], while here the excitations have been found up to approximately 18 meV with $E_i = 21.91$ meV. Whether there are spin excitations at even higher energies need to be further studied. Similar to previous results [36], the low-energy spin excitations at (2/3,0) and the symmetrical positions gradually merge together at the zone center (1,0) below about 8 meV. At higher energies, new excitations emerge from the zone corners, i.e., (2/3,2/3) and (4/3,-2/3), as further shown in Fig. 3(c). These locations correspond to the K points in the Brillouin zone [see the inset of Fig. 4(a)]. When the energy increases to about 15 meV, the spin excitations are observed throughout the Brillouin zone [Fig. 3(d)]. Note that the $|Q|$ dependence of the intensity at 15 meV can be fitted by a cosine function analogous to the structure factor of randomly arranged nearest-neighbour singlets together with the magnetic form factor of Cu^{2+} [44], which results in seemingly higher intensities at smaller Q's.

Previous Raman scattering has revealed high-energy magnetic excitations that are suggested to come from one-pair (1P) and two-pair (2P) spinon-antispinon excitations [41]. Here, we plot the intensity of our high-energy spin excitations together with the 1P Raman susceptibility in the A_{1g} channel in Fig. 4(a). Note that we have combined the neutron data at different temperatures since the high-energy spin excitations are essentially temperature-independent for the temperature range measured here ($T \leq 6$ K). A broad peak is found in neutron scattering data at about 14 meV at the K point, similar to the peak in Raman 1P excitations, suggesting their common origin. Note that the Raman scattering technique detects spinon-antispinon pairs with a total spin quantum number $\Delta S = 0$, while INS measures two spinon excitations with $\Delta S = \pm 1$ [49]. The probability of two excited spinons with the same and opposite spin quantum numbers could be same so that the results of Raman and neutron scattering are consistent, and there seems no reason why they might be different. These excitations also exist at the M and K' points, but

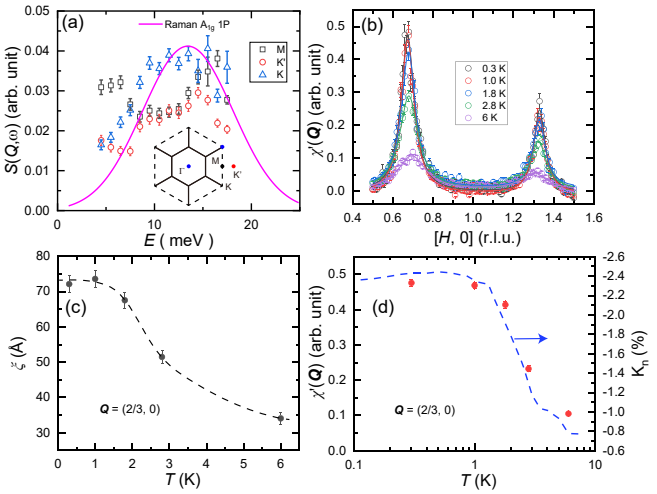

FIG. 4. (a) Energy dependence of $S(Q,\omega)$ above 4 meV. The solid line represents Raman magnetic susceptibility for 1P spinon-antispinon excitations in the A_{1g} channel [41]. The inset shows kagome (solid lines) and extended (dashed lines) Brillouin zones with high-symmetry points. (b) $\chi'(Q)$ along the [H,0] direction at several temperatures. The solid lines are fitted results by the Lorentzian function. (c) Temperature dependence of magnetic correlation length ξ at Q = (2/3,0). The dashed line is a guide to the eye. (d) Temperature dependence of $\chi'(Q)$ at Q = (2/3,0). The dashed blue line is the Knight shift from the NMR measurements [35].

are significantly enhanced with decreasing energy compared with Raman susceptibility. Note that Raman spectroscopy only detects signal at Γ (Q =0), so its results cannot be directly compared with the low-energy spin excitations measured by the INS technique at finite Q's.

As shown previously, we can obtain the real part of the dynamical susceptibility $\chi'(Q)$ from the Kramers-Kronig relationship [36]. Figure 4(b) shows $\chi'(Q)$ along the [H,0] direction at various temperatures. The peaks at (2/3,0) and (4/3,0) become much broader and lower at 6 K compared to those at low temperatures. The magnetic correlation length ξ at (2/3,0) can be calculated as $\xi = 2\pi/w$, where w is the full width at half maximum (FWHM) of the $\chi'(Q)$ peak at (2/3,0) fitted by the Lorentzian function. Figure 4(c) shows the temperature dependence of ξ, which increases with decreasing T and saturates below about 1 K. This seems to accord with the loss of T^2 dependence in the specific heat above 1 K [31, 44]. Figure 4(d) shows the temperature dependence of the peak intensity $\chi'(Q)$ at (2/3,0), which also becomes saturated below about 1 K. Note that the Knight shift $^{81}K_n$ obtained from the nuclear magnetic resonance (NMR) spectroscopy shows similar behavior [35].

We start the discussions with two major arguments against the existence of Dirac QSL in the YCu_3-Br system. The first argument is that the magnetic susceptibility and Knight shift do not decrease linearly with decreasing temperature when T approaches zero or increase linearly with increasing field at very low temperatures, which is expected for a Dirac QSL since they are supposed to be proportional to the density of states [31, 35, 39]. However, this assumption is true only when the spin rotation symmetry is preserved. In our sample, the observation of anisotropy between in-plane and out-of-plane spin excitations suggest that the spin system is not a pure Heisenberg one. Theoretical calculations have shown that the dynamical spin structure factor of quantum spin liquids becomes anisotropic in the presence of DM interaction [8, 50]. Experimental evidence for the existence of out-of-plane DM interaction has been found in a very similar material, $YCu_3(OH)_6Cl_3$, with an AFM order [51], which is consistent with our observation $M_{ab} > M_c$ [8]. Therefore, the anisotropic spin excitations in our sample clearly demonstrate the existence of c-axis DM interaction, which may have randomness due to structural disorders in this system [30, 32, 36, 37]. The magnetic susceptibility or Knight shift can no longer be considered effective tools to probe the ground states, as it has long been known that when the spin rotation symmetry is absent, the magnetic susceptibility tends to a constant at zero temperature, irrespective of the nature of low-energy excitations [1]. It is worth noting that the existence of DM interaction might be crucial for generating gauge field in this system [52].

The second argument against the Dirac QSL is the absence of linear temperature dependence of thermal conductivity under fields [33]. A gap value of 1.4 K (≈ 0.12 meV) has been suggested but is larger than the lowest energy of spin excitations in this work (≈ 0.05 meV). As pointed out in our previous work [36], to observe linear-T thermal conductivity, κ, the mean free path, l, should be at least several tens of microns, according to $\kappa = C\nu_F l/3$, where C is the specific heat and ν_F is the spinon velocity, in the order of 1 km/s. While it is obviously hard to fulfill such a requirement in a system with disorders [30, 32, 36–38], we can estimate the mean free path using our INS data. As shown above, we have observed a linear temperature dependence of the FWHM of low-energy spin excitations. The broadening of spin excitations in reciprocal space is typically due to the decrease of magnetic correlations. This seems to suggest a divergence of correlation length [44], which contradicts the simple fact that there is no indication of any magnetic order at zero K and ξ actually saturates below about 1 K [Fig. 4(c)]. On the other hand, the spinon-spinon interaction can naturally cause the broadening of spin excitations. It is well known that the inverse inelastic quasiparticle lifetime τ^{-1} near the Dirac nodes in the intrinsic undoped graphene is linear with both temperature and energy due to electron-electron interaction [53]. We argue that the same mechanism may also work for Dirac spinons, so the energy width ΔE of the Dirac dispersion is linear with both temperature and energy, too, as $\Delta E \sim \tau^{-1}\hbar/2$. Because INS experiments detect two-spinon excitations, the

momentum width ΔQ at low energies is also linear with temperature as $\Delta E \sim \hbar\nu_F\Delta Q$, where ν_F is the spinon velocity. While this argument might be too simple and the instrument resolution should be considered to fully reproduce the experimental data, the estimated values should be reasonable within an order or two. The mean free path is thus in the order of tens of nanometers at low temperatures, as $l = \nu_F\tau$, clearly much smaller than the minimum requirement in thermal transport measurements (tens of microns [36]).

Our results provide a rare example to directly compare INS data with Raman and NMR results in QSL candidates, as shown in Figs. 4(a) and 4(d), respectively. The consistency between the Knight shift and $\chi'[(Q = (2/3, 0)]$ confirms the dominant contribution of excitations at (2/3,0) at very low energies. Compared to Raman scattering, our INS data revealed Q dependence of the high-energy spin excitations, which seems to emerge from the K positions in the extended Brillouin zone. The low-energy spin excitations cannot be described by the conventional kagome AFM model and their locations are consistent with the so-called Q=(1/3,1/3) magnetic order [54, 55]. On the other hand, the spin waves in the latter also merge into the zone center of the kagome Brillouin, i.e., Q = (1,0), at about 8 meV, but no damped magnons should exist above it, further supporting the origin of the spin excitations above 8 meV as pairs of spinons. The high-energy spin excitations are consistent with theoretical calculations based on the kagome AFM model [8, 50, 56], where the intensity at K is higher than that at M when the energy is much larger than J. Note that these calculations have uncertainties in one way or another so more theoretical studies are needed.

In conclusion, our results provide further evidence for the Dirac QSL in YCu_3-Br. The linear temperature dependence of the low-energy spin excitations suggests the existence of spinon-spinon interactions, analogous to those of Dirac electrons in graphene. Polarized INS reveals anisotropic low-energy spin excitations due to the existence of DM interactions. High-energy excitations provide evidence for the existence of spinon pairs that are consistent with kagome AFM model, although the low-energy spin excitations seem not. These results provide a harmonious picture across different experimental techniques and call for further theoretical studies.

S. L. thanks Y. Zhou, Z. Y. Meng, and K. Jiang for helpful discussions. This work is supported by the National Key Research and Development Program of China (Grants No. 2022YFA1403400, No. 2021YFA1400400,2023YFA1406100), the Chinese Academy of Sciences (Grants No. XDB33000000, No. GJTD-2020-01). Measurements on AMATERAS were performed based on the approved proposal (Grant No. 2023B0063).

L.H. and Z.Z. contributed equally to this work.

* kenji.nakajima@j-parc.jp
† y.su@fz-juelich.de
‡ slli@iphy.ac.cn

[1] L. Savary and L. Balents, Quantum spin liquids: A review, Rep. Prog. Phys. **80**, 016502 (2017).
[2] Y. Zhou, K. Kanoda, and T.-K. Ng, Quantum spin liquid states, Rev. Mod. Phys. **89**, 025003 (2017).
[3] C. Broholm, R. J. Cava, S. A. Kivelson, D. G. Nocera, M. R. Norman, and T. Senthil, Quantum spin liquids, Science **367**, 263 (2020).
[4] M. B. Hastings, Dirac structure, RVB, and Goldstone modes in the kagomé antiferromagnet, Phys. Rev. B **63**, 014413 (2000).
[5] M. Hermele, Y. Ran, P. A. Lee, and X.-G. Wen, Properties of an algebraic spin liquid on the kagome lattice, Phys. Rev. B **77**, 224413 (2008).
[6] Y.-C. He, M. P. Zaletel, M. Oshikawa, and F. Pollmann, Signatures of dirac cones in a dmrg study of the kagome heisenberg model, Phys. Rev. X **7**, 031020 (2017).
[7] W. Zhu, X. Chen, Y.-C. He, and W. Witczak-Krempa, Entanglement signatures of emergent Dirac fermions: Kagome spin liquid and quantum criticality, Sci. Adv. **4**, eaat5535 (2018).
[8] W. Zhu, S. shu Gong, and D. N. Sheng, Identifying spinon excitations from dynamic structurefactor of spin-1/2 Heisenberg antiferromagnet onthe kagome lattice, Proc. Natl. Acad. Sci. U.S.A **116**, 5437 (2019).
[9] X.-Y. Song, C. Wang, A. Vishwanath, and Y.-C. He, Unifying description of competing orders in two-dimensional quantum magnets, Nat. Commun. **10**, 4254 (2019).
[10] M. Hering, J. Sonnenschein, Y. Iqbal, and J. Reuther, Characterization of quantum spin liquids and their spinon band structures via functional renormalization, Phys. Rev. B **99**, 100405 (2019).
[11] E. Dupuis, M. B. Paranjape, and W. Witczak-Krempa, Transition from a dirac spin liquid to an antiferromagnet: Monopoles in a qed_3-gross-neveu theory, Phys. Rev. B **100**, 094443 (2019).
[12] X.-Y. Song, Y.-C. He, A. Vishwanath, and C. Wang, From spinon band topology to the symmetry quantum numbers of monopoles in Dirac spin liquids, Phys. Rev. X **10**, 011033 (2020).
[13] Y. Iqbal, F. Ferrari, A. Chauhan, A. Parola, D. Poilblanc, and F. Becca, Gutzwiller projected states for the $J_1 - J_2$ heisenberg model on the kagome lattice: Achievements and pitfalls, Phys. Rev. B **104**, 144406 (2021).
[14] D. Kiese, F. Ferrari, N. Astrakhantsev, N. Niggemann, P. Ghosh, T. Müller, R. Thomale, T. Neupert, J. Reuther, M. J. P. Gingras, S. Trebst, and Y. Iqbal, Pinch-points to half-moons and up in the stars: The kagome skymap, Phys. Rev. Res. **5**, L012025 (2023).
[15] F. Ferrari, F. Becca, and R. Valentí, Spin-phonon interactions on the kagome lattice: Dirac spin liquid versus valence-bond solids, Phys. Rev. B **109**, 165133 (2024).
[16] U. F. P. Seifert, J. Willsher, M. Drescher, F. Pollmann, and J. Knolle, Spin-peierls instability of the U(1) Dirac spin liquid, Nat. Commun. **15**, 7110 (2024).
[17] M. A. de Vries, K. V. Kamenev, W. A. Kockelmann, J. Sanchez-Benitez, and A. Harrison, Magnetic ground state of an experimental $S = 1/2$ kagome antiferromagnet, Phys. Rev. Lett. **100**, 157205 (2008).

[18] D. E. Freedman, T. H. Han, A. Prodi, P. Müller, Q.-Z. Huang, Y.-S. Chen, S. M. Webb, Y. S. Lee, T. M. McQueen, and D. G. Nocera, Site specific x-ray anomalous dispersion of the geometrically frustrated kagomé magnet, herbertsmithite, $ZnCu_3(OH)_6Cl_2$, J. Am. Chem. Soc. **132**, 16185 (2010).

[19] Y. Y. Huang, Y. Xu, L. Wang, C. C. Zhao, C. P. Tu, J. M. Ni, L. S. Wang, B. L. Pan, Y. Fu, Z. Hao, C. Liu, J.-W. Mei, and S. Y. Li, Heat transport in herbertsmithite: Can a quantum spin liquid survive disorder?, Phys. Rev. Lett. **127**, 267202 (2021).

[20] T. H. Han, J. S. Helton, S. Chu, D. G. Nocera, J. A. Rodriguez-Rivera, C. Broholm, and Y. S. Lee, Fractionalized excitations in the spin-liquid state of a kagome-lattice antiferromagnet, Nature **492**, 406 (2012).

[21] M. Fu, T. Imai, T.-H. Han, and Y. S. Lee, Evidence for a gapped spin-liquid ground state in a kagome heisenberg antiferromagnet, Science **350**, 655 (2015).

[22] T.-H. Han, M. R. Norman, J.-J. Wen, J. A. Rodriguez-Rivera, J. S. Helton, C. Broholm, and Y. S. Lee, Correlated impurities and intrinsic spin-liquid physics in the kagome material herbertsmithite, Phys. Rev. B **94**, 060409 (2016).

[23] P. Khuntia, M. Velazquez, Q. Barthélemy, F. Bert, E. Kermarrec, A. Legros, B. Bernu, A. Z. L. Messio, and P. Mendels, Gapless ground state in the archetypal quantum kagome antiferromagnet $ZnCu_3(OH)_6Cl_2$, Nat. Phys. **16**, 469 (2020).

[24] Z. Feng, Z. Li, X. Meng, W. Yi, Y. Wei, J. Zhang, Y.-C. Wang, W. Jiang, Z. Liu, S. Li, F. Liu, J. Luo, S. Li, G. qing Zheng, Z. Y. Meng, J.-W. Mei, and Y. Shi, Gapped spin-1/2 spinon excitations in a new kagome quantum spin liquid compound $Cu_3Zn(OH)_6FBr$, Chin. Phys. Lett. **34**, 077502 (2017).

[25] Y. Wei, Z. Feng, W. Lohstroh, D. H. Yu, D. Le, C. dela Cruz, W. Yi, Z. F. Ding, J. Zhang, C. Tan, L. Shu, Y.-C. Wang, H.-Q. Wu, J. Luo, J.-W. Mei, F. Yang, X.-L. Sheng, W. Li, Y. Qi, Z. Y. Meng, Y. Shi, and S. Li, Evidence for the topological order in a kagome antiferromagnet, arXiv e-prints , arXiv:1710.02991 (2017), arXiv:1710.02991 [cond-mat.str-el].

[26] Z. Feng, W. Yi, K. Zhu, Y. Wei, S. Miao, J. Ma, J. Luo, S. Li, Z. Y. Meng, and Y. Shi, From claringbullite to a new spin liquid candidate $Cu_3Zn(OH)_6FCl$, Chin. Phys. Lett. **36**, 017502 (2018).

[27] Y. Fu, M.-L. Lin, L. Wang, Q. Liu, L. Huang, W. Jiang, Z. Hao, C. Liu, H. Zhang, X. Shi, J. Zhang, J. Dai, D. Yu, F. Ye, P. A. Lee, P.-H. Tan, and J.-W. Mei, Dynamic fingerprint of fractionalized excitations in single-crystalline $Cu_3Zn(OH)_6FBr$, Nature Communications **12**, 3048 (2021).

[28] Y. Wei, X. Ma, Z. Feng, Y. Zhang, L. Zhang, H. Yang, Y. Qi, Z. Y. Meng, Y.-C. Wang, Y. Shi, and S. Li, Nonlocal effects of low-energy excitations in quantum-spin-liquid candidate $Cu_3Zn(OH)_6FBr$, Chin. Phys. Lett. **38**, 097501 (2021).

[29] M. R. Norman, Colloquium: Herbertsmithite and the search for the quantum spin liquid, Rev. Mod. Phys. **88**, 041002 (2016).

[30] X.-H. Chen, Y.-X. Huang, Y. Pan, and J.-X. Mia, Quantum spin liquid candidate $YCu_3(OH)_6Br_2[Br_x(OH)_{1-x}]$ ($x \approx 0.51$): With an almost perfect kagomé layer, J. Magn. Magn. Mater. **512**, 167066 (2020).

[31] Z. Zeng, X. Ma, S. Wu, H.-F. Li, Z. Tao, X. Lu, X.-h. Chen, J.-X. Mi, S.-J. Song, G.-H. Cao, G. Che, K. Li, G. Li, H. Luo, Z. Y. Meng, and S. Li, Possible Dirac quantum spin liquid in the kagome quantum antiferromagnet $YCu_3(OH)_6Br_2[Br_x(OH)_{1-x}]$, Phys. Rev. B **105**, L121109 (2022).

[32] J. Liu, L. Yuan, X. Li, B. Li, K. Zhao, H. Liao, and Y. Li, Gapless spin liquid behavior in a kagome heisenberg antiferromagnet with randomly distributed hexagons of alternate bonds, Phys. Rev. B **105**, 024418 (2022).

[33] X. Hong, M. Behnami, L. Yuan, B. Li, W. Brenig, B. Büchner, Y. Li, and C. Hess, Heat transport of the kagome Heisenberg quantum spin liquid candidate $YCu_3(OH)_{6.5}Br_{2.5}$: Localized magnetic excitations and a putative spin gap, Phys. Rev. B **106**, L220406 (2022).

[34] F. Lu, L. Yuan, J. Zhang, B. Li, Y. Luo, and Y. Li, The observation of quantum fluctuations in a kagome Heisenberg antiferromagnet, Commun. Phys. **5**, 272 (2022).

[35] S. Li, Y. Cui, Z. Zeng, Y. Wang, Z. Hu, J. Liu, C. Li, X. Xu, Y. Chen, Z. Liu, S. Li, and W. Yu, Nmr evidence of spinon localization in the kagome antiferromagnet $YCu_3(OH)_6Br_2[Br_{1-x}(OH)_x]$, Phys. Rev. B **109**, 104403 (2024).

[36] Z. Zeng, C. Zhou, H. Zhou, L. Han, R. Chi, K. Li, M. Kofu, K. Nakajima, Y. Wei, W. Zhang, D. G. Mazzone, Z. Y. Meng, and S. Li, Spectral evidence for dirac spinons in a kagome lattice antiferromagnet, Nat. Phys. **20**, 1097 (2024).

[37] A. Xu, Q. Shen, B. Liu, Z. Zeng, L. Han, L. Yan, J. Luo, J. Yang, R. Zhou, and S. Li, Magnetic ground states in the kagome system $ycu_3(OH)_6[(Cl_xBr_{1-x})_{3-y}(OH)_y]$, Phys. Rev. B **110**, 085146 (2024).

[38] B. S. Shivaram, J. C. Prestigiacomo, A. Xu, Z. Zeng, T. D. Ford, I. Kimchi, S. Li, and P. A. Lee, Nonanalytic magnetic response and intrinsic ferromagnetic clusters in a kagome spin-liquid candidate, Phys. Rev. B **110**, L121105 (2024).

[39] S. Suetsugu, T. Asaba, S. Ikemori, Y. Sekino, Y. Kasahara, K. Totsuka, B. Li, Y. Zhao, Y. Li, Y. Kohama, and Y. Matsuda, Gapless spin excitations in a quantum spin liquid state of s=1/2 perfect kagome antiferromagnet (2024), arXiv:2407.16208.

[40] S. Suetsugu, T. Asaba, Y. Kasahara, Y. Kohsaka, K. Totsuka, B. Li, Y. Zhao, Y. Li, M. Tokunaga, and Y. Matsuda, Emergent spin-gapped magnetization plateaus in a spin-1/2 perfect kagome antiferromagnet, Phys. Rev. Lett. **132**, 226701 (2024).

[41] S. Jeon, D. Wulferding, Y. Choi, S. Lee, K. Nam, K. H. Kim, M. Lee, T.-H. Jang, J.-H. Park, S. Lee, S. Choi, C. Lee, H. Nojiri, and K.-Y. Choi, One-ninth magnetization plateau stabilized by spin entanglement in a kagome antiferromagnet, Nat. Phys. **20**, 435 (2024).

[42] G. Zheng, Y. Zhu, K.-W. Chen, B. Kang, D. Zhang, K. Jenkins, A. Chan, Z. Zeng, A. Xu, O. A. Valenzuela, J. Blawat, J. Singleton, P. A. Lee, S. Li, and L. Li, Unconventional magnetic oscillations in kagome Mott insulators (2023), arXiv:2310.07989.

[43] G. Zheng, D. Zhang, Y. Zhu, K.-W. Chen, A. Chan, K. Jenkins, B. Kang, Z. Zeng, A. Xu, D. Ratkovski, J. Blawat, A. Bangura, J. Singleton, P. A. Lee, S. Li, and L. Li, Thermodynamic evidence of fermionic behavior in the vicinity of one-ninth plateau in a kagome antiferromagnet (2024), arXiv:2409.05600.

[44] See Supplemental Materials.

[45] K. Nakajima, S. Ohira-Kawamura, T. Kikuchi, M. Nakamura, R. Kajimoto, Y. Inamura, N. Takahashi, K. Aizawa, K. Suzuya, K. Shibata, T. Nakatani, K. Soyama, R. Maruyama, H. Tanaka, W. Kambara, T. Iwahashi, Y. Itoh, T. Osakabe, S. Wakimoto, K. Kakurai, F. Maekawa, M. Harada, K. Oikawa, R. E. Lechner, F. Mezei, and M. Arai, AMATERAS: A cold-neutron disk chopper spectrometer, J. Phys. Soc. Jpn. **80**, SB028 (2011).

[46] M. Boehm, A. Hiess, J. Kulda, S. Roux, and J. Saroun, ThALES—three axis low energy spectroscopy at the Institut Laue–Langevin, Meas. Sci. Technol. **19**, 034024 (2008).

[47] Y. Inamura, T. Nakatani, J. Suzuki, and T. Otomo, Development status of software 'Utsusemi' for chopper spectrometers at MLF, J-PARC, J. Phys. Soc. Jpn. **82**, SA031 (2013).

[48] L. P. Regnault, Inelastic neutron polarization analysis, in *Neutron Scattering from Magnetic Materials*, edited by T. Chatterji (Elsevier B.V., 2006) Chap. 8, pp. 363–395.

[49] Strictly speaking, it is not clear whether neutron scattering can detect two spinon excitations with a total $S = 0$ or not, but the argument in the text holds in both cases.

[50] F. Ferrari, S. Niu, J. Hasik, Y. Iqbal, D. Poilblanc, and F. Becca, Static and dynamical signatures of Dzyaloshinskii-Moriya interactions in the heisenberg model on the kagome lattice, SciPost Phys. **14**, 139 (2023).

[51] T. Arh, M. Gomilšek, P. Prelovšek, M. Pregelj, M. Klanjšek, A. Ozarowski, S. J. Clark, T. Lancaster, W. Sun, J.-X. Mi, and A. Zorko, Origin of magnetic ordering in a structurally perfect quantum kagome antiferromagnet, Phys. Rev. Lett. **125**, 027203 (2020).

[52] B. Kang and P. A. Lee, Generation of gauge magnetic fields in a kagome spin liqud candidate using the Dzyaloshinskii-Moriya interaction (2024), arXiv:2401.01946.

[53] Q. Li and S. Das Sarma, Finite temperature inelastic mean free path and quasiparticle lifetime in graphene, Phys. Rev. B **87**, 085406 (2013).

[54] D. Chatterjee, P. Puphal, Q. Barthélemy, J. Willwater, S. Süllow, C. Baines, S. Petit, E. Ressouche, J. Ollivier, K. M. Zoch, C. Krellner, M. Parzer, A. Riss, F. Garmroudi, A. Pustogow, P. Mendels, E. Kermarrec, and F. Bert, From spin liquid to magnetic ordering in the anisotropic kagome Y-kapellasite $Y_3Cu_9(OH)_{19}Cl_8$: A single-crystal study, Phys. Rev. B **107**, 125156 (2023).

[55] M. Hering, F. Ferrari, A. Razpopov, I. I. Mazin, R. Valentí, H. O. Jeschke, and J. Reuther, Phase diagram of a distorted kagome antiferromagnet and application to Y-kapellasite, npj Comput. Mater. **8**, 10 (2022).

[56] M. Punk, D. Chowdhury, and S. Sachdev, Topological excitations and the dynamic structure factor of spin liquids on the kagome lattice, Nat. Phys. **10**, 289 (2014).